Monthly Notices
of the
ROYAL ASTRONOMICAL SOCIETY

MNRAS **482,** 5275–5289 (2019)
Advance Access publication 2018 November 3

doi:10.1093/mnras/sty2991

Chemical analysis of K giants in the young open cluster NGC 2345

N. Holanda [1]★ C. B. Pereira[1] and N. A. Drake[1,2,3]

[1] *Observatório Nacional/MCTIC, Rua Gen. José Cristino 77, 20921-400 Rio de Janeiro, Brazil*
[2] *Laboratory of Observational Astrophysics, Saint Petersburg State University, Universitetski pr. 28, Petrodvoretz 198504, Saint Petersburg, Russia*
[3] *Laboratório Nacional de Astrofísica, Rua Estados Unidos 154, 37504-364 Itajubá, Brazil*

Accepted 2018 October 31. Received 2018 October 31; in original form 2018 September 17

ABSTRACT

We present results for the elemental abundances of five K giants of the young open cluster NGC 2345. The atmospheric parameters of the studied giants and their chemical abundances were determined using high-resolution optical spectroscopy. In this study, we determine abundances of light elements (Li, C, N), light odd-Z elements (Na, Al), α-elements (Mg, Si, Ca, Ti), Fe-group elements (Cr, Fe, Ni), and n-capture elements (Y, Zr, La, Ce, Nd, Sm, Eu) for each star. Abundances of the light elements and Eu were obtained using spectral synthesis technique. Also, rotation velocities were determined through the spectral synthesis of the Fe I line at 6151.6 Å. The mean metallicity obtained for the open cluster is [Fe/H] $= -0.33 \pm 0.05$ and it is considered low compared to recent studies for open clusters in the Milky Way, although low for its Galactic latitude ($b = -02\overset{\circ}{.}31$). Lastly, the abundance analysis shows that there is good agreement with the profile of field clump stars with the same metallicity.

Key words: stars: abundances – stars: fundamental parameters – open clusters and associations: individual: NGC 2345.

1 INTRODUCTION

In stellar open clusters we can assume that all the stars are formed in the same interstellar cloud at roughly the same time, at the same distance and with similar chemical composition, making them excellent laboratories for the study of stellar and Galactic evolution (see Friel 1995; da Silveira, Pereira & Drake 2018, among others). In particular, young open clusters are excellent tracers of spiral structure and are helpful tools to study recent star formation in Milky Way, because they are indicators of the variations in the abundance of heavy chemical elements in the Galactic disc (Lada & Lada 2003). Nevertheless, the precise measurement of elemental abundances required spectroscopic observations at high resolution, which are available only for about 10 per cent of the currently known open clusters (Heiter et al. 2014).

In this paper, we focus on the open cluster NGC 2345, a young open cluster, with an age of 0.079 Gyr, using high-resolution spectroscopy with the aim to obtain its abundance pattern of its known member stars. NGC 2345 is located in Canis Majoris (ℓ, b) = ($226\overset{\circ}{.}58$, $-02\overset{\circ}{.}31$) at a distance of 2.251 kpc (Kharchenko et al. 2005), being slightly younger than the Pleiades. The cluster contains five bright K-type giants, one of them is in a binary system. The first report of the NGC 2345 highlights the presence of seven luminous stars at a distance of 10 kpc (Stephenson & Sanduleak 1971). Later, Moffat (1974) made *UBV* photometry and a spectroscopic observation yield for NGC 2345 a distance of 1.75 kpc and an age of 60 Myr, denoting the existence of five red giants and two blue bright giants. In this study by Moffat, the spectrum analysis of #34 reveals that it is formed of two stars, one red giant and other (probably) subgiant star of B type. Fig. 1 shows the stellar field of NGC 2345. Following the same strategy as for our previous studies for open clusters (e.g. Santrich, Pereira & Drake 2013; Sales Silva et al. 2014; da Silveira et al. 2018; Peña-Suárez et al. 2018), we observed all the known giant stars that belong to the cluster according to Mermilliod, Mayor & Udry (2008).

Previous spectroscopic analysis done for this cluster showed that it has a surprisingly low metallicity ([Fe/H] $= -0.26 \pm 0.03$) for a thin-disc cluster (Reddy, Lambert & Giridhar 2016). In addition, being very young, NGC 2345 should be composed by massive stars. In fact, as it will be seen, it has a turn-off mass of 5.4 $M_\odot$. Low metallicity among massive stars is not usually found as can be seen in fig. 3 of Takeda, Sato & Murata (2008) and fig. 17 of Zieliński et al. (2012). In fact, the two most massive stars from the sample of 322 giants analysed by Takeda et al. (2008) have masses of, respectively, 4.91 and 4.99 $M_\odot$ with metallicities, respectively, of +0.08 and −0.02, while from the sample of 348 giants analysed by Zieliński et al. (2012) the most massive star has a mass of 3.4 $M_\odot$ with a metallicity of −0.18. Therefore, NGC 2345 is a useful target for a high-resolution spectroscopy analysis in order to probe possible effects of mixing and dredge-up events in massive stars and to search for a relationship between abundance ratios and age for a comparison with older clusters.

It is interesting that other massive clusters, such as NGC 1545 (Začs et al. 2011) and NGC 5316 (Drazdauskas et al. 2016) with

★ E-mail: nacizoholanda@on.br

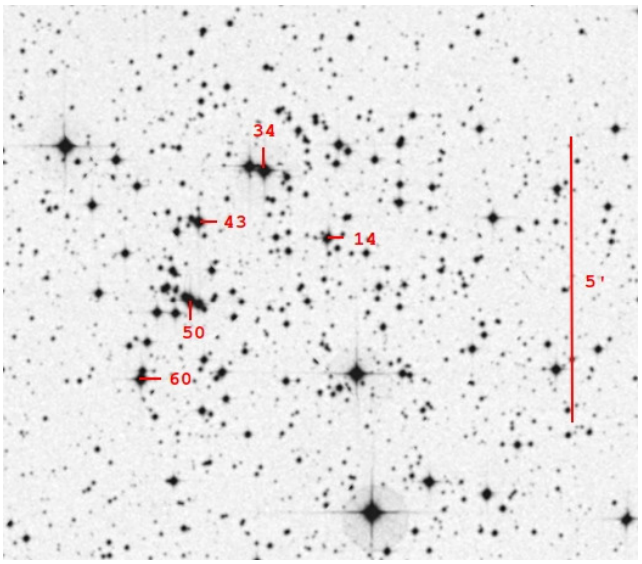

Figure 1. Finding chart for stars spectroscopically observed in the field of NGC 2345 (DSS2 blue image from CDS portal). Stars are marked according to ID provided Moffat (1974).

ages of 0.09 and 0.08 Gyr and Galactocentric distances estimated as 8.59 and 7.4 kpc, respectively, are in a good agreement with the radial Galactic gradient. Unlike NGC 2345 presents a metallicity below the pattern found in clusters at the same distance and/or with a similar turn-off mass. Another cluster, NGC 3105 (Alonso-Santiago et al. 2018), with stars having masses around 10 $M_{\odot}$, also has a similar low metallicity ([Fe/H] $= -0.29$), is closer to the radial Galactic gradient pattern than NGC 2345, which is much less massive.

As above mentioned, we used high-resolution spectroscopy to determine the atmospheric parameters and abundances for several chemical elements for the four single red giants and one spectroscopic binary for the K giant in NGC 2345. The abundances of the light elements (lithium, carbon, and nitrogen), europium, and the $^{12}C/^{13}C$ isotopic ratio were determined using spectral synthesis technique, while the abundances of Na, Mg, Al, Ca, Si, Ti, Ni, Cr, Y, Zr, La, Ce, Nd, and Sm were determined using equivalent width measurements. The oxygen abundance was not possible to determine because of the contamination of by telluric lines. In addition, we also determined rotational velocities of the stars in this cluster. There are a few determinations of the rotational velocities of the giants in open clusters, especially in those young clusters. Therefore, determining rotation rates may set important constraints for a binary system and also for the physical mechanism of dredge-up of angular momentum from a fast rotating core in a single star (Santrich et al. 2013).

2 OBSERVATIONS

The observations were carried out using Échelle spectrograph Fiber-fed Extended Range Optical Spectrograph (FEROS; Kaufer et al. 1999) at the 2.2-m Max Planck Gesellschaft/European Southern Observatory (ESO) Telescope in La Silla, Chile. The FEROS provides a full wavelength coverage of 3800–9200 Å with resolving power $R = 48\,000$, corresponding to 2.2 pixels of 15 μm. The exposure time of our spectra ranges from 1200 to 2400 s to achieve a typical signal-to-noise ratio (S/N) = 100–150 (individual values are given in Table 1). All spectra were reduced with the FEROS Data Reduction System pipeline.

In order to complement the spectroscopic data, we used the *UBV* photometry of Moffat (1974), downloading it from the WEBDA data base.[1] Once we have done this, we employed the isochrone fitting method to determine the age of NGC 2345 as shown in Fig. 2. We adopted a colour excess of $E(B-V) = 0.616$ (Dias et al. 2002).

Table 1 gives the basic information of the observed stars. The stars were selected from the radial velocity survey of Mermilliod et al. (2008). The radial velocities obtained for all stars analysed in this study are also shown in Table 1. From these data for four stars we obtain a mean radial velocity for the cluster as $\langle RV \rangle = 58.49 \pm 0.41\,km\,s^{-1}$, which is in good agreement with 59.11 ± 1.31 and $57.70 \pm 0.42\,km\,s^{-1}$ reported by Mermilliod et al. (2008) and Reddy et al. (2016), respectively. To calculate the mean, the star #34 was excluded due to its binary nature. In addition, Table 1 shows the rotation velocities obtained for the stars analysed in this work.

In Fig. 3, we plot the turn-off mass versus age for some clusters including NGC 2345. From the isochrone fit, we derived a turn-off mass of $5.40 \pm 0.15\,M_{\odot}$ and an age of $\log t = 7.9 \pm 0.1$ (or 79.4 Myr). This value is in agreement with the values of $\log t = 7.85$ and $\log t = 7.74$ reported by Dias et al. (2002) and Kharchenko et al. (2005), respectively.

3 ANALYSIS AND RESULTS

3.1 Atmospheric parameters

Atmospheric parameters of the stars analysed in this work were determined using the standard spectroscopic method and line list provided by Hekker & Meléndez (2007). This list is composed of 20 Fe I and six Fe II lines between 5700 and 7800 Å. This line list is appropriate for an analysis of cool giants, avoiding line blending from CN bands (Meléndez & Barbuy 1999; Santos et al. 2009). In Table A1, we show the equivalent widths of the Fe I and Fe II lines used to determine the atmospheric parameters. The equivalent widths were obtained by fitting Gaussian profiles to the observed ones using the task SPLOT in IRAF.[2] The red giants analysed by us have a cool limit of 4000 K and a hot limit of 4850 K. We used local thermodynamical equilibrium (LTE) plane-parallel atmospheric models of (Kurucz (1993)) and the spectral analysis code MOOG (Sneden 1973) for the determination of stellar atmospheric parameters. The effective temperature ($T_{\rm eff}$) was obtained requiring that the abundance of Fe I lines (in the notation $[X/H] = \log(N_X/N_H)_{\star} - \log(N_X/N_H)_{\odot}$) did not depend on the lower level excitation potential (χ). The surface gravities ($\log g$) were determined from the iron ionization equilibrium. The microturbulence velocity (ξ) was found requiring that the abundance of Fe I lines did not depend on the reduced equivalent width ($\log(W_{\lambda}/\lambda)$).

Determining these three main parameters through multiple iterations provides us with the value of metallicity as calculated from the used Fe I lines. We compare the derived spectroscopic gravities with the evolutionary gravities $\log g_{\star}$ using the turn-off mass ($M_{\rm turn\text{-}off}$)

[1]Site dedicated to open star clusters and is the web version of the data base known as BDA. Available on http://webda.physics.muni.cz/.
[2]The Image Reduction and Analysis Facility is written and supported by the National Optical Astronomy Observatories (NOAO). Available at http://iraf.noao.edu/.

Table 1. Basic information of the observed stars in NGC 2345. Star number, V, $(B-V)$, and radial velocities (RV) were taken from Moffat (1974)[a], Mermilliod et al. (2008)[b], and Reddy et al. (2016)[c] are shown in columns 1–6. The rotational velocities are shown in column 7. The last two columns provide the date of observation and the exposure times.

Star	V^a	$(B-V)^a$	RV (km s^{-1})	RV^b (km s^{-1})	RV^c (km s^{-1})	$v \sin i$ (km s^{-1})	Observation date	Exp (s)
#14	10.73	2.06	58.96 ± 0.41	59.8 ± 0.40	–	4.5 ± 0.4	2016 Mar 11	2400
#34	9.94	1.50	64.23 ± 0.44	61.18 ± 0.74	63.60 ± 0.40	10.1 ± 0.4	2016 Mar 11	1200
#43	10.70	1.81	58.43 ± 0.52	58.82 ± 0.27	58.00 ± 0.40	4.7 ± 0.6	2016 Mar 11	2400
#50	10.40	2.04	58.61 ± 0.60	60.41 ± 0.40	–	5.2 ± 0.4	2016 Mar 11	1500
#60	10.48	1.82	57.97 ± 0.52	58.41 ± 0.35	57.40 ± 0.30	5.8 ± 0.4	2016 Mar 11	1500

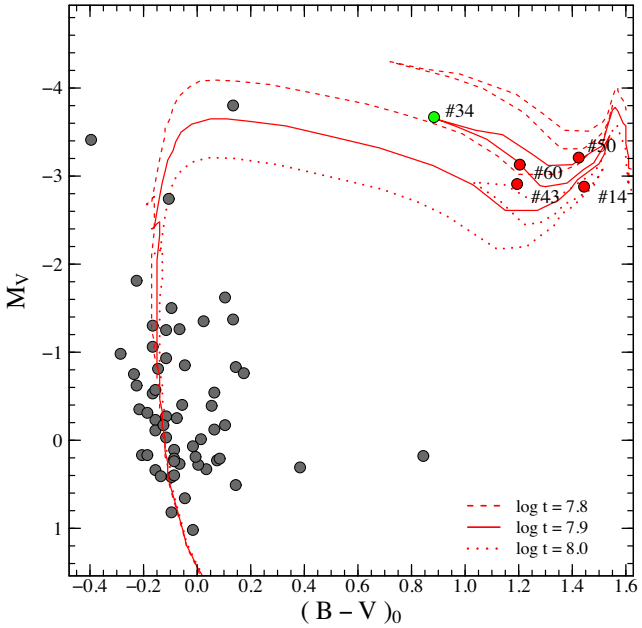

Figure 2. Reddening-corrected colour–magnitude diagram of NGC 2345 with photometric data taken from Moffat (1974). Our program stars are identified by red filled circles (singles) and green filled circle (binary). We also show isochrones (Bertelli et al. 1994) for elements three different ages: 63.09 Myr ($\log t = 7.8$), 79.43 Myr ($\log t = 7.9$), and 100 Myr ($\log t = 8.0$).

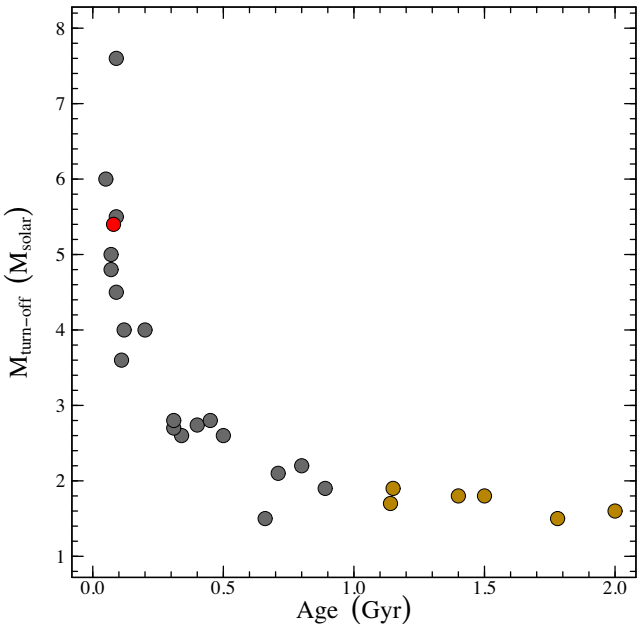

Figure 3. Turn-off mass versus age for open clusters and NGC 2345 (the red circle). According to Friel (1995), young clusters have age less than 1.0 Gyr (grey circles) and old clusters have age more than 1.0 Gyr (dark yellow circles).

obtained from the isochrone fittings using the equation

$$\log g_\star = \log\left(\frac{M_{\text{turn-off}}}{M_\odot}\right) + 0.4\,(V - A_V + \text{BC}_V) + 4\log T_{\text{eff}} - 2\log r\,(\text{kpc}) - 16.5.$$

In the equation above, V, A_V, and BC_V are, respectively, the visual magnitude, interstellar absorption in V band, and bolometric correction. The surface gravity, mass, and temperature of the star are, respectively, $\log g_\star$, $M_\star$, and T_{eff} and r is the heliocentric distance of the open cluster given in kpc. The solar parameters atmospheric used in this equation are $M_{\text{bol}} = 4.75$, $\log g = 4.44$, and $T_{\text{eff}} = 5777$ K, as well the bolometric corrections were calculated using the relation given in Alonso, Arribas & Martínez-Roger (1999). In addition, we adopted the distances of *Gaia* Data Release 2 (Gaia Collaboration et al. 2018) and $A_V = 1.909$ (Dias et al. 2002). The result of confronting spectroscopic and photometric gravities gave us a mean difference of -0.03 ± 0.22. The results for all the five giants are given in Table 2, as well as the photometric and spectroscopic $\log \frac{L}{L_\odot}$.

The errors in the atmospheric parameters, effective temperature, and microturbulent velocity were estimated from the uncertainties in the slopes of relationships A(Fe I) versus χ and A(Fe I) versus W_λ/λ, respectively. In addition, the standard deviation in the Fe I abundance was used to provide the uncertainty in the $\log g$ parameter. In these procedures, we find uncertainties of $\Delta T_{\text{eff}} = \pm 70$–$100$, $\Delta \log g = \pm 0.1$–0.2, and $\Delta \xi = \pm 0.15$–0.3.

3.2 Abundances analysis

Two techniques were employed to derive the chemical abundances: equivalent width measurements and spectral synthesis. We used equivalent width measurements for the determination of the abundances for Na, Mg, Al, Si, Ca, Ti, Cr, Ni, Y, La, Ce, Nd, and Sm. The adopted line list was the same of our previous papers. All lines were inspected and some of them were excluded due to blending, hence the final line list differs slightly from star to star. As for the determination of the atmospheric parameters, we used LTE model atmospheres of Kurucz (1993) and the code MOOG for the abundance determinations of the elements above mentioned. In addition, the abundances of the elements were normalized using the solar abundances of Asplund et al. (2009). Table A2 shows the atomic lines used for the determination of the chemical abundances.

The abundances of the light elements (lithium, carbon, and nitrogen), the $^{12}C/^{13}C$ isotopic ratio, and europium were determined in the same way as in da Silveira et al. (2018) using the same line

Table 2. Adopted spectroscopic atmospheric parameters and luminosity for the giant stars of NGC 2345. In addition, we also show the photometric temperature, gravity, and luminosity, respectively, in the notation of $T_{\rm eff}$, $\log g$, and $\log \frac{L}{L_\odot}$.

Star	$T_{\rm eff}^{\rm spec}$ (K)	$\log g^{\rm spec}$	ξ (km s^{-1})	[Fe I/H] $\pm \sigma$	[Fe II/H] $\pm \sigma$	$\log \frac{L}{L_\odot}^{\rm spec}$	$T_{\rm eff}^{\rm phot}$ (K)	$\log g^{\rm phot}$	$\log \frac{L}{L_\odot}^{\rm phot}$
#14	4150	1.10	2.36	-0.33 ± 0.09	-0.34 ± 0.13	3.78	3877	1.03	3.85
#34	4850	1.10	3.00	-0.26 ± 0.12	-0.24 ± 0.06	4.05	4843	1.29	3.86
#43	4350	1.60	2.45	-0.32 ± 0.07	-0.31 ± 0.07	3.36	4250	1.35	3.61
#50	4000	0.70	2.31	-0.37 ± 0.10	-0.37 ± 0.10	4.12	3881	1.01	3.81
#60	4020	1.03	2.54	-0.39 ± 0.08	-0.38 ± 0.10	3.80	4185	0.99	3.84

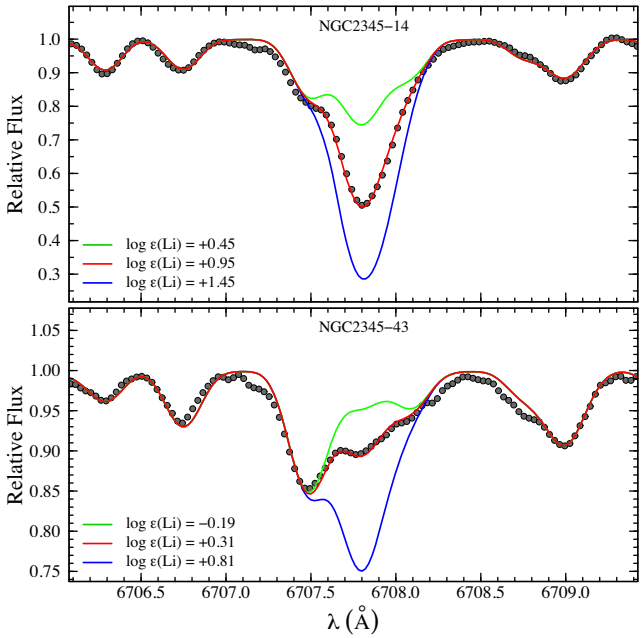

Figure 4. Observed (dotted line) and synthetic (solid lines) spectra in the region around the Li I line at λ6708 Å line for the stars #14 and #43.

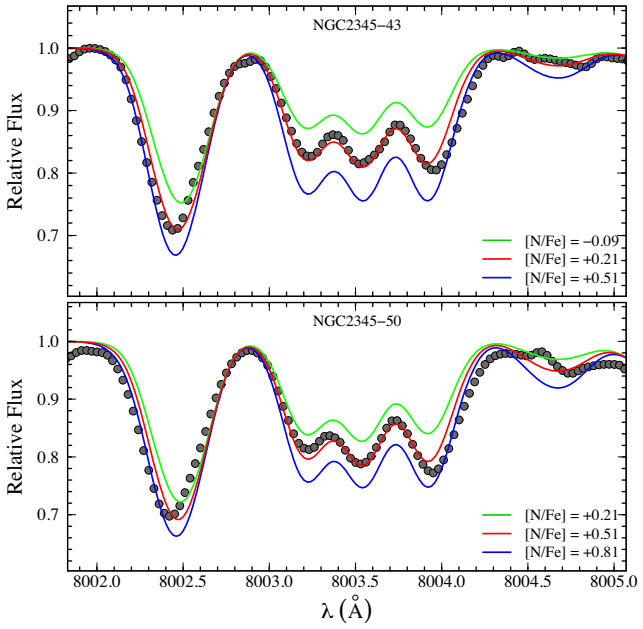

Figure 5. Observed (dotted line) and synthetic (solid lines) spectra between 8002 and 8005 Å for the stars #43 and #50.

list for the same spectral regions for the spectral synthesis. The abundance of carbon was determined using the spectral region of the C_2 molecule [C_2 (0,1) band head of the Swan system $A^3\Pi_g - X^3\Pi_u$ at 5635 Å]. The electron oscillator strength, $f_{\rm el} = 0.033$, was taken from Lambert (1978). The Hönl–London factors for the rotational lines were calculated using formula from Kovács (1969). Franck–Condon factors were calculated according to Dwivedi et al. (1978). C_2 dissociation energy of $D_0(C_2) = 6.15$ eV was adopted (Huber & Herzberg 1979). The wavelengths of the C_2 features of the (0,1) band were taken from Phillips & Davis (1968).

The nitrogen abundance was obtained by comparing the observed and theoretical line profiles for the ^{12}CN lines of the (2, 0) band of the CN red system $A^2\Pi - X^2\Sigma$ in the 7994–8020 Å wavelength range. Oscillator strength of the (0,2) band $f_{2,0} = 8.4 \times 10^{-4}$ (Sneden & Lambert 1982) was used. Hönl–London factors were calculated using Schadee (1964) formula. The dissociation energy $D_0(CN) = 7.65$ eV was used (Bauschlicher, Langhoff & Taylor 1988; Lambert 1994). The wavelengths of the ^{12}CN lines were taken from Davis & Phillips (1963) and those of ^{13}CN lines from Wyller (1966).

The europium abundance was determined using the Eu II line at λ6645.13 Å and the hyperfine splitting was taken from Mucciarelli et al. (2008).

Unfortunately, we could not obtain the oxygen abundance based on the forbidden line at 6300 Å because of the contamination with

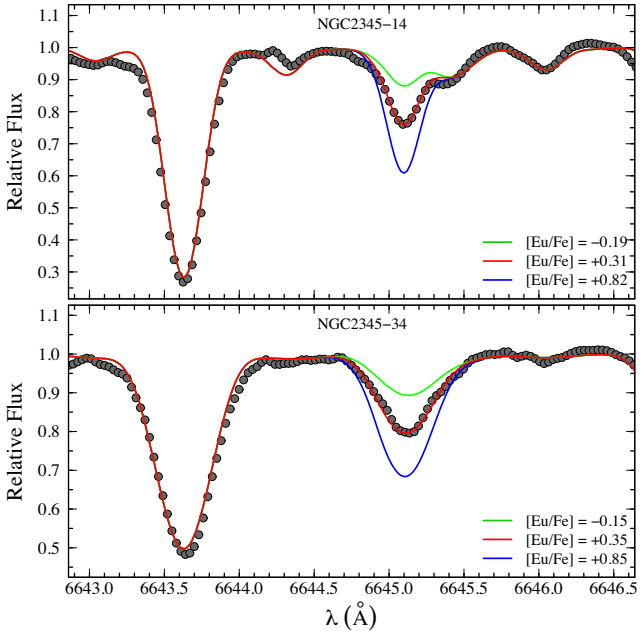

Figure 6. Observed (dotted line) and synthetic spectra (solid lines) in the region around the Eu II line at λ6645.13 Å line for the stars #14 and #34.

Table 3. Light element abundances and $^{12}C/^{13}C$ isotopic ratios.

Star	log ϵ (Li)	[C/Fe]	[N/Fe]	$^{12}C/^{13}C$
#14	+0.95	+0.02	+0.62	>24
#34	+0.11	− 0.05	+0.65	18
#43	+0.31	+0.26	+0.21	>30
#50	+0.81	+0.11	+0.51	>26
#60	+0.19	+0.13	+0.63	>30
Mean	+0.47 ± 0.34	+0.09 ± 0.12	+0.52 ± 0.18	>25.6

telluric O_2 lines. Therefore, we assumed a [O/Fe] ratio of +0.12 since the oxygen abundance affects the carbon abundance. Figs 4–6 show, respectively, the observed and synthetic spectra for the stars NGC 2345 – 14 and 43 around the lithium line at 6708 Å, the observed and synthetic spectra for the stars NGC 2345 – 43 and 50 between 8002 and 8005 Å for CN lines, and the observed and synthetic spectra for the stars NGC 2345 – 14 and 34 around the europium line at 6645 Å. Tables 3 and 4 show all results of the abundance determinations and the obtained mean cluster abundance. The lithium abundance is given in the notation $\log \varepsilon(\mathrm{Li}) = \log [N_{\mathrm{Li}}/N_{\mathrm{H}}] + 12$. We also provide the mean abundance, s, of the elements created by the s-process (Y, Zr, La, Ce, and Nd) in the notation [s/Fe].

3.2.1 Abundance uncertainties

Tables 5 and 6 show the influence of the uncertainties of the atmospheric parameters over the chemical abundances for the star #34. In addition, in Table 5 we also show the abundance variation due to the uncertainty of 3.0 mÅ in the equivalent width of the observed lines for each chemical specie, considering the FEROS spectral resolution and the S/N (Cayrel 1988) around 100. The seventh column provides the total abundance uncertainty calculated as the root square of the sum of the various sources of uncertainties. The last column of Table 5 provides the abundance dispersion between the lines for each element with more than available lines. Overall, inspecting Table 5 reveals that neutral species exhibit higher sensitivity to temperature variation, while ionized species exhibit the greater differences due to the uncertainties in the surface gravities. In addition to carbon and nitrogen abundances, the uncertainties in carbon abundance affect the nitrogen abundance and vice versa once we used CN molecular lines for its determination.

4 DISCUSSION

4.1 Rotation velocities

The determination of the rotational velocities $v \sin i$ was made by using spectral synthesis for the Fe I 6151.6 Å line. We fixed macroturbulent velocity as 3.0 km s^{-1} (Fekel 1997) for all stars and also considering the instrumental broadening for the FEROS spectral resolution. The instrumental broadening was determined measuring the Gausssian full width at half-maximum of the thorium–argon lines used for the wavelength calibration for FEROS spectrograph. Table 1 shows rotational velocities for giants of the open cluster NGC 2345, while Fig. 7 shows the synthesis for the Fe I 6151.6 Å line for stars #34 and #60 with different values of $v \sin i$. The best fits for these stars are the rotational velocities of 10.1 and 5.8 km s^{-1} (red solid lines), respectively. The mean projected rotational velocity for NGC 2345 is 5.05 ± 0.58 (excluding the binary star #34). This value is close to the mean value of 4.5 ± 1.2 km s^{-1} for 1288 single giant stars with $v \sin i < 9.0$ km s^{-1} studied by Carlberg et al. (2011).

Fig. 8 shows the temperature distribution as a function of the projected rotational velocity obtained from Carlberg et al. (2011) (grey circles), consider the star with $v \sin i < 20.0$ km s^{-1}. The stars of our sample are shown as red circles and the binary #34 as green circles with photometric (triangles) and spectroscopic (circles) derived temperatures. This comparison reveals the good agreement between the spectroscopic and photometric derived temperatures for stars of NGC 2345.

4.2 The abundance pattern

4.2.1 Metallicity

NGC 2345 presents the mean metallicity of −0.33 ± 0.05 (based on the abundance given by the Fe I lines). This result is slightly different from the result given by Reddy et al. (2016), as previously mentioned. Reddy et al. (2016) used three giants (#34, #43, and #60) and found a mean metallicity of −0.26 ± 0.03. Using the same three stars we obtained a mean metallicity of −0.32 ± 0.06.

Like most of the chemical elements in the thin-disc stars, the abundance of iron also decreases with the Galactocentric distance. The radial Galactic gradient shown in Fig. 9 highlights this atypical metallicity of NGC 2345. The linear regression (red dashed line) was done based only on the distribution of the Cepheids and has a slope −0.06 dex kpc^{-1} (Genovali et al. 2014). In addition, young open clusters were included for a closer comparison are shown as grey circles using data from Netopil et al. (2016) and distances taken from WEBDA. The grey triangle represents NGC 3105 (Alonso-Santiago et al. 2018), which has a metallicity and a Galactocentric distance (10 kpc) similar to that of NGC 2345. The linear fit (blue dashed line) for the clusters distribution presents a slope of −0.08 dex kpc^{-1} ($R_{\mathrm{GC}} \leq 12.0$ kpc), which are in good agreement with −0.09 dex kpc^{-1} derived by Yong, Carney & Friel (2012). It is important to note the existence of a discontinuity in the Galactic metallicity gradient at 12.0–13.0 kpc (Yong et al. 2012), which is the so-called transition radius between the inner and outer disc. The inner disc has a more pronounced gradient, while the metallicity gradient of the outer disc is almost flat. Another observation, concerning to the thick-disc clusters in this analysis, shows that the profile of the gradient becomes smoother, as observed in fig. 4 presented by Reddy et al. (2016).

The Galactocentric distances projected to the Galactic plane were calculated based on the distances of the cluster to the Sun (d), Galactic longitudes (l), and latitudes (b), with the well-known relation

$$R_{\mathrm{GC}}^2 = \mathrm{R}_{\odot}^2 + (d \cos b)^2 - 2\,\mathrm{R}_{\odot}\, d \cos l \cos b,$$

where $\mathrm{R}_{\odot}$ is the Galactocentric distance of the Sun that we assume as 7.95 kpc, rescaling the data compiled by Netopil et al. (2016) to Genovali et al. (2014). The distance of 2.251 kpc (Kharchenko et al. 2005) was used to determine the Galactocentric radius for our cluster, $R_{\mathrm{GC}} = 9.64$ kpc.

4.2.2 Light elements: Li, C, N, and the $^{12}C/^{13}C$ isotopic ratio

When a star reaches the red giant branch, the increase of the convective envelope dilutes the ^{7}Li (among other species such as ^{12}C, ^{16}O, and ^{18}O) and reduces significantly its surface abundance. Therefore, it is expected to find a typical lithium abundance in the range $-1.0 < \log \varepsilon(\mathrm{Li}) < 1.0$ (Gilroy 1989; Charbonnel & Balachandran 2000). In good agreement with this scenario of the first dredge-up,

Table 4. Abundance ratios [X/Fe] and the standard deviations for the targets in NGC 2345.

[X/Fe]	#14	#34	#43	#50	#60	⟨[X/Fe]⟩
[Na I/Fe]	+0.40 (3)	+0.28 (2)	+0.10 (4)	+0.34 (3)	+0.21 (2)	+0.27 ± 0.12
[Mg I/Fe]	+0.09 (5)	+0.10 (2)	+0.21 (3)	+0.26 (3)	+0.22 (4)	+0.18 ± 0.08
[Al I/Fe]	+0.17 (3)	+0.18 (4)	+0.09 (4)	+0.13 (4)	+0.09 (5)	+0.13 ± 0.04
[Si I/Fe]	+0.28 (6)	+0.18 (4)	+0.31 (1)	+0.28 (7)	+0.41 (4)	+0.29 ± 0.08
[Ca I/Fe]	− 0.03 (3)	+0.05 (4)	− 0.03 (3)	+0.01 (2)	+0.02 (3)	+0.00 ± 0.04
[Ti I/Fe]	0.00 (4)	+0.10 (9)	− 0.05 (7)	+0.08 (4)	–	+0.03 ± 0.07
[Cr I/Fe]	+0.06 (11)	− 0.04 (8)	+0.03 (15)	+0.03 (7)	− 0.04 (7)	+0.01 ± 0.04
[Ni I/Fe]	− 0.05 (6)	− 0.06 (12)	− 0.06 (9)	− 0.05 (11)	− 0.06 (5)	− 0.06 ± 0.01
[Y II/Fe]	+0.29 (3)	+0.16 (2)	+0.26 (3)	+0.30 (3)	+0.19 (2)	+0.24 ± 0.06
[Zr I/Fe]	+0.10 (12)	+0.11 (5)	+0.04 (11)	+0.06 (12)	− 0.10 (8)	+0.04 ± 0.08
[La II/Fe]	+0.53 (5)	+0.50 (3)	+0.53 (5)	+0.41 (4)	+0.35 (4)	+0.46 ± 0.08
[Ce II/Fe]	+0.28 (4)	+0.20 (4)	+0.35 (4)	+0.21 (4)	+0.05 (6)	+0.22 ± 0.11
[Nd II/Fe]	+0.35 (5)	+0.41 (10)	+0.41 (7)	+0.22 (8)	+0.20 (11)	+0.32 ± 0.10
[Sm II/Fe]	+0.28 (4)	+0.21 (3)	+0.38 (3)	0.11 (3)	− 0.04 (4)	+0.19 ± 0.16
[Eu II/Fe]	+0.31 (1)	+0.35 (1)	+0.41 (1)	+0.26 (1)	+0.28 (1)	+0.32 ± 0.06
[α/Fe]	+0.08	+0.11	+0.11	+0.16	+0.22	+0.14 ± 0.05
[s/Fe]	+0.31	+0.28	+0.32	+0.24	+0.14	+0.26 ± 0.07

Table 5. Abundance uncertainties for NGC 2345 – 34. From the second to the fourth column we show the variations of abundances caused by the variations of the atmospheric parameters. The fifth column refers to the variation of abundances due to metallicity. The sixth column provides the uncertainty due to a variation of 3.0 mÅ in the equivalent width of each measured line. In seventh column we present the total compounded rms uncertainty of the second to the sixth columns. Finally, the last column provides the standard deviation among the abundances given by individual lines for elements with more than three available lines.

Species	Δ $T_{\rm eff}$ (K) +90 K	Δlog g +0.2	Δξ +0.3 km s^{-1}	Δ[Fe/H] +0.12 dex	ΔEW +3 mÅ	$(\Sigma\,\sigma^2)^{1/2}$	$\sigma_{\rm obs}$
Li I	+0.00	+0.05	− 0.10	− 0.01	–	+0.11	–
Na I	+0.07	− 0.01	− 0.04	+0.00	+0.03	+0.09	+0.03
Mg I	+0.03	+0.00	+0.05	− 0.01	+0.03	+0.07	+0.11
Al I	+0.05	− 0.01	+0.03	− 0.01	+0.03	+0.07	+0.14
Si I	+0.02	− 0.02	− 0.04	+0.01	+0.04	+0.06	+0.09
Ca I	+0.07	− 0.02	− 0.05	− 0.01	+0.04	+0.10	+0.06
Ti I	+0.13	− 0.01	+0.04	− 0.01	+0.03	+0.14	+0.13
Cr I	+0.08	− 0.02	− 0.03	− 0.01	+0.04	+0.10	+0.19
Fe I	+0.10	+0.00	− 0.04	+0.01	+0.04	+0.12	+0.13
Fe II	− 0.07	+0.09	− 0.10	+0.03	+0.03	+0.16	+0.06
Ni I	+0.10	+0.00	+0.05	+0.00	+0.03	+0.12	–
Y II	− 0.01	+0.06	− 0.05	+0.04	+0.04	+0.10	–
Zr I	+0.16	− 0.02	+0.00	+0.00	+0.07	+0.18	+0.15
La II	+0.00	+0.08	− 0.04	+0.03	+0.03	+0.10	+0.02
Ce II	+0.00	+0.08	− 0.04	+0.04	+0.04	+0.11	+0.07
Nd II	+0.01	+0.08	− 0.07	+0.03	+0.03	+0.11	+0.23
Sm II	+0.02	+0.07	− 0.07	+0.03	+0.04	+0.11	+0.10
Eu II	+0.00	+0.10	− 0.10	+0.10	–	+0.17	–

Table 6. Influence of the errors in atmospheric parameters over the abundances of lithium, carbon, and nitrogen for NGC 2345 – 34. We also give the dependence of the uncertainty of carbon abundance over the nitrogen abundance and vice versa.

Species	Δ$T_{\rm eff}$ (K) +90 K	Δlog g +0.2	Δξ +0.3 km s^{-1}	Δlog (C) +0.20 dex	Δlog (N) +0.20 dex	Δlog (O) +0.20 dex	$(\Sigma\sigma^2)^{1/2}$
C (C_2)	+0.00	− 0.05	−0.05	–	−0.10	+0.05	+0.13
N (CN)	+0.05	+0.00	−0.05	−0.20	–	+0.10	+0.23

the abundance of lithium is low in the giants studied here. The mean value for the lithium abundance for the stars of our sample is 0.47 ± 0.34, which can be considered overabundant with respect to NGC 2451 ($\log \varepsilon(\mathrm{Li}) = -0.50$) and Cr 140 ($\log \varepsilon(\mathrm{Li}) = 0.15$), which have similar turn-off masses of ∼6.0 and ∼5.0 $M_\odot$, respectively (Gilroy 1989). We raise for the need for more new studies in order to obtain lithium abundances in open clusters, in particular in young clusters. Recent study done by Delgado-Mena et al. (2016) is essential, but it was concentrated on stars with 'higher' gravities (those with $\log g > 2.0$). For a faithful compari-

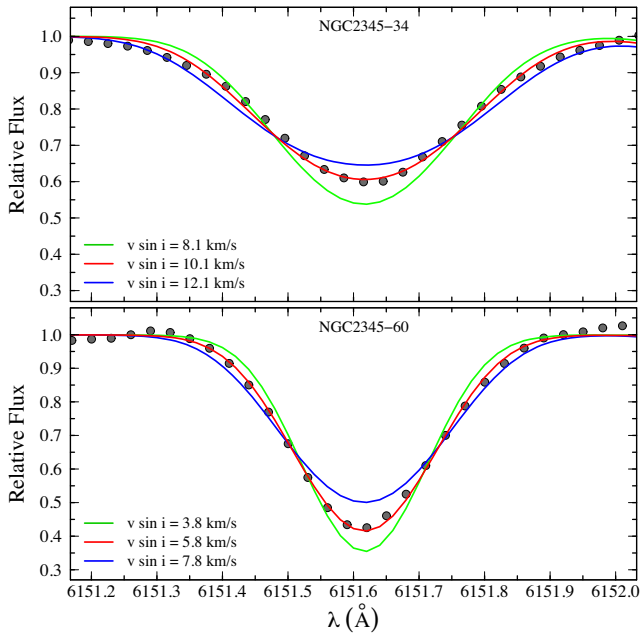

Figure 7. Observed (black dots) and synthetic spectra in the region of the Fe I line at 6151.6 Å for giants #34 and #60 of the open cluster NGC 2345. The figure shows the three absorption profiles corresponding to the different rotational velocities.

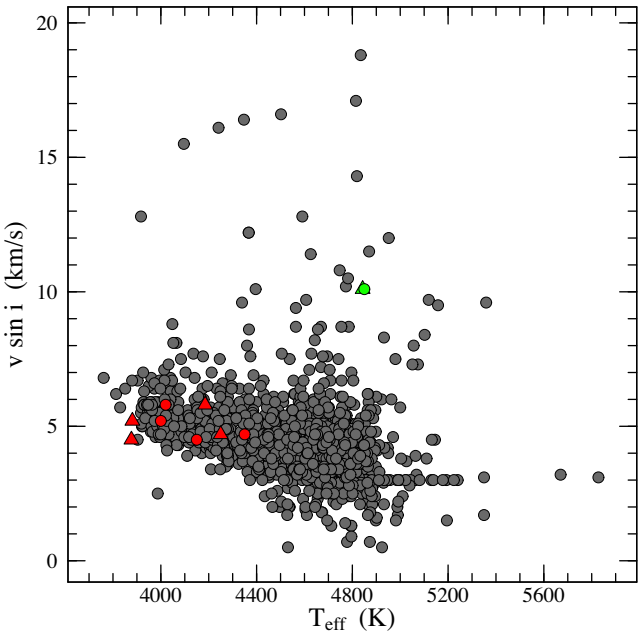

Figure 8. Projected rotational velocities and photometric temperature for giants stars. The grey circles represent the stars from the sample studied by Carlberg et al. (2011). Circles and triangles denote, respectively, the spectroscopic and photometric temperatures. Red symbols represent the single stars and green the binary star NGC 2345 – 34.

son with NGC 2345, for example, stars with $\log g \leq 1.5$ would be required.

In Fig. 10, we show our derived [C/Fe] and [N/Fe] ratios in comparison with the same ratios obtained by Mishenina et al. (2006) and Luck & Heiter (2007) (abundances normalized to Asplund et al. 2009) for disc red clump giants and local disc field giants. The

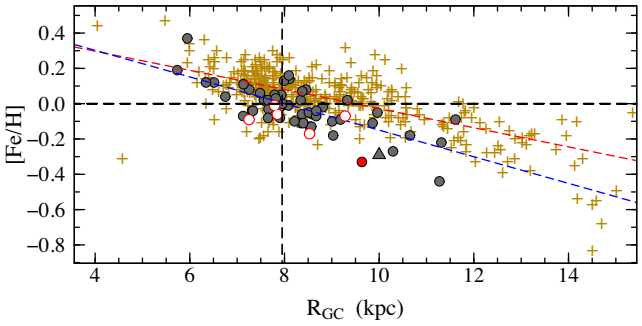

Figure 9. The average [Fe/H] versus Galactocentric distance with iron abundance gradients of -0.06 dex kpc^{-1} (red dashed line; Genovali et al. 2014) and -0.08 dex kpc^{-1} (blue dashed line) for Cepheids and open clusters, respectively. The yellow crosses represent Cepheids studied by Genovali et al. (2013, 2014) and other sources used by them. The grey filled circles represent young open clusters ($\leq$1 Gyr) with metallicities determined through high-resolution spectroscopy and compiled by Netopil et al. (2016). The grey triangle represents to NGC 3105 studied by Alonso-Santiago et al. (2018).

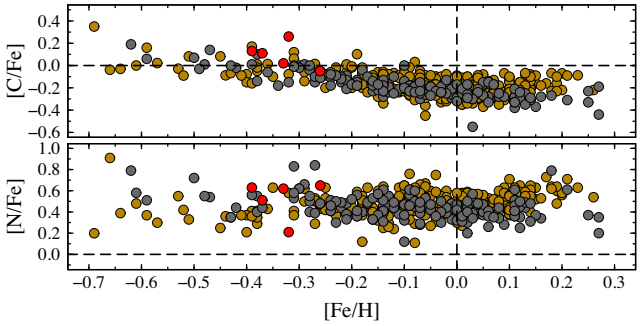

Figure 10. Abundance ratios [X/Fe] versus [Fe/H] for carbon and nitrogen. The red circles represent the giants analysed in this work, while the dark yellow circles represent the abundances reported by Luck & Heiter (2007) and the grey circles represent the abundances reported by Mishenina et al. (2006). The dashed lines indicate the solar value.

results for [C/Fe] and [N/Fe] ratios for the five giants analysed in this work, show first dredge-up profile, as can be seen in Table 3. As mentioned before, abundance of ^{12}C is reduced as a consequence of the first dredge-up process and, the abundance of ^{14}N increased (Karakas & Lattanzio 2014), as is clearly observed in all the stars analysed.

The ^{12}C/^{13}C isotope ratio is a useful evolutionary indicator for low- and intermediate-mass stars because it is a tracer of which nuclear processes occur inside these objects. Fig. 11 shows the ^{12}C/^{13}C ratio predicted for giants at first dredge-up with standard and thermohaline extra-mixing and thermohaline and rotation-induced mixing for evolutionary models calculated by Charbonnel & Lagarde (2010) and Lagarde et al. (2012). We use data from several sources of the literature in the range $1.58 \leq M_{\text{turn-off}} \leq 5.6$. When we compare the mean of ^{12}C/^{13}C ratio obtained for the giants of NGC 2345 with the values predicted by mixing models, it is possible to verify that the best agreement is for the standard model of first dredge-up by Lagarde et al. (2012). However, our ^{12}C/^{13}C ratio is not low enough to be in agreement with the thermohaline and rotation-induced mixing model calculated by Lagarde et al. (2012), as was observed in the open clusters analysed by Peña-Suárez et al. (2018) (diamonds) and Santrich et al. (2013) (circle). A similar

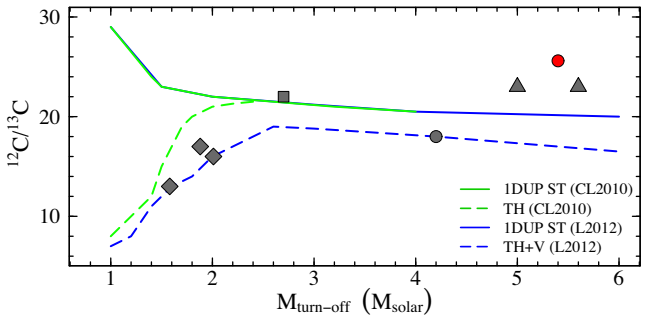

Figure 11. $^{12}C/^{13}C$ versus $M_{turn-off}$ in clump stars of open clusters. NGC 2345 is represented by red circle. The grey triangles represent the mean of the $^{12}C/^{13}C$ ratio for NGC 4609 and NGC 5316 (Drazdauskas et al. 2016), the grey circle for NGC 3114 (Santrich et al. 2013), the grey square for NGC 2447 (da Silveira et al. 2018), and the grey diamonds for NGC 2360, NGC 3680, and NGC 5822 (Peña-Suárez et al. 2018). The solid green and blue lines represent the $^{12}C/^{13}C$ isotopic ratio predicted for giants at first dredge-up with standard evolutionary models for solar metallicity calculated, respectively, by Charbonnel & Lagarde (2010) and Lagarde et al. (2012). The green dashed line represents the prediction for thermohaline extra-mixing calculated by Charbonnel & Lagarde (2010). Finally, the blue dashed line represents the prediction for thermohaline and rotation-induced mixing calculated by Lagarde et al. (2012).

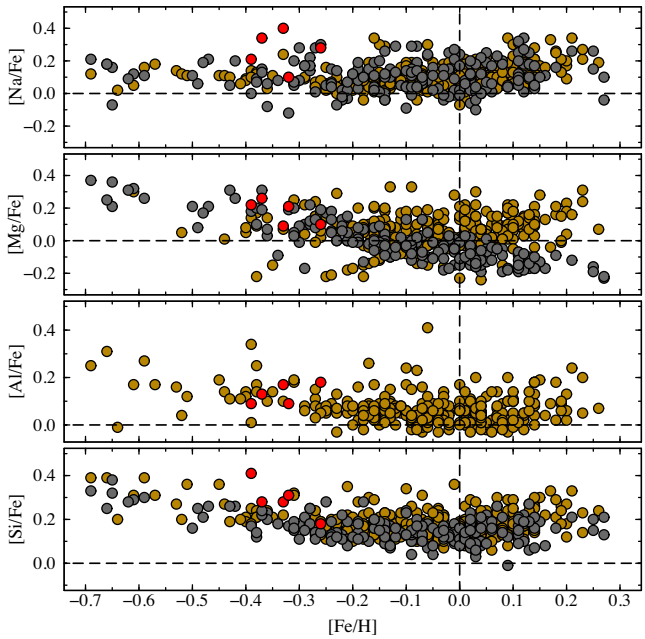

Figure 12. Abundance ratios [X/Fe] versus [Fe/H] for the elements from Na to Si. Symbols have the same meaning as in Fig. 10.

fact was observed by Drazdauskas et al. (2016) in their study of clusters NGC 4609 and NGC 5316, with $M_{turn-off}$ values similar to NGC 2345.

4.2.3 Other elements: Na to Ni

Figs 12 and 13 show the abundances of the elements from sodium to nickel for the giant stars of the NGC 2345 in comparison with

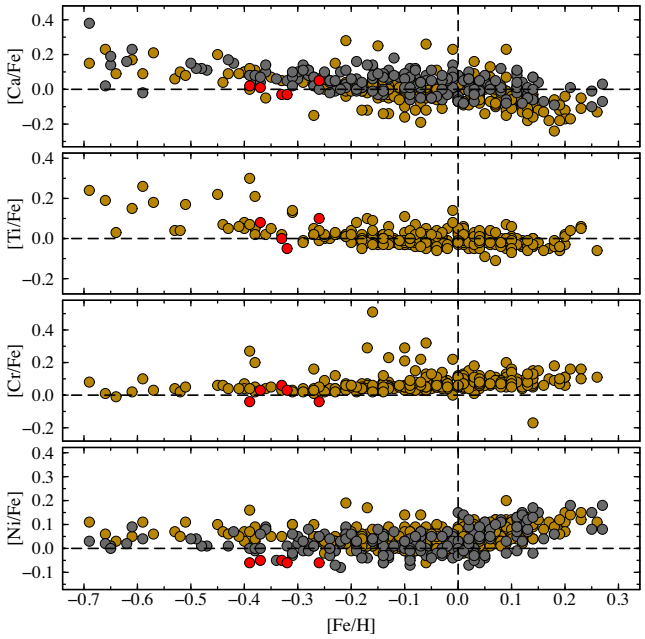

Figure 13. Abundance ratios [X/Fe] versus [Fe/H] for the elements from Ca to Ni. Symbols have the same meaning as in Fig. 10.

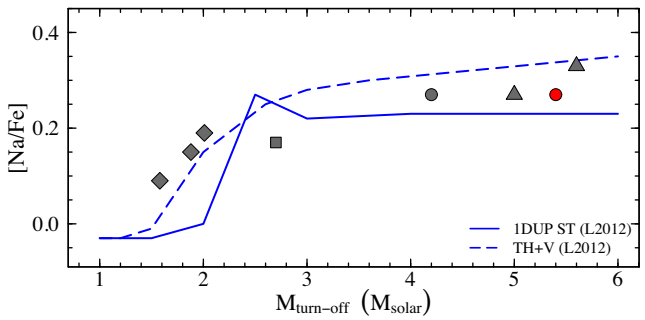

Figure 14. Mean [Na/Fe] ratio versus $M_{turn-off}$ for NGC 2345 (red circle) and open cluster of literature. The symbols and models (Lagarde et al. 2012) compared have the same meaning as those in Fig. 11. However, it is worth nothing that the sodium abundances used for Santrich et al. (2013) and Drazdauskas et al. (2016) were determined via NTLE.

field stars. The mean abundance found for [Na/Fe] by Reddy et al. (2016) is close to our result. For example, we determined the mean abundance of $+0.27 \pm 0.12$, while Reddy et al. (2016) estimated at $+0.18 \pm 0.02$.

Sodium is also an element sensitive to the first dredge-up and other extra-mixing processes, especially in intermediate-mass stars (for the Galactic disc metallicities). Fig. 14 shows the theoretical models by Lagarde et al. (2012) for the first dredge-up for a standard stellar evolutionary model (solid line) and thermohaline mixing and rotation-induced mixing model (dashed line). Similar to the $^{12}C/^{13}C$ isotopic ratio, the value found for sodium-over-iron approximates to the standard stellar evolutionary model at first dredge-up and shows less agreement with the prediction given by thermohaline and rotation-induced mixing.

The mean of α-elements over iron, defined as $[\alpha/Fe] = \frac{1}{4}([Mg\,I/Fe]+[Si\,I/Fe]+[Ca\,I/Fe]+[Ti\,I/Fe])$ for the five giants, is $+0.14 \pm 0.05$ (Table 4). This result is in agreement with local disc field giants. Comparatively, the mean value for the [α/Fe] ratio for

Table 7. Abundance ratios [X/Fe] for the elements from sodium to nickel for NGC 2345 determined in this work in comparison with the same elements analysed by Reddy et al. (2016). The mean presented by Reddy et al. (2016) was based on the abundances of the stars #34, #43, and #60.

Species	This work	Reddy et al. (2016)
[Na I/Fe]	$+0.27 \pm 0.12$	$+0.18 \pm 0.02$
[Mg I/Fe]	$+0.18 \pm 0.08$	$+0.05 \pm 0.03$
[Al I/Fe]	$+0.13 \pm 0.04$	$+0.03 \pm 0.02$
[Si I/Fe]	$+0.29 \pm 0.08$	$+0.25 \pm 0.02$
[Ca I/Fe]	$+0.00 \pm 0.04$	-0.13 ± 0.03
[Ti I/Fe]	$+0.03 \pm 0.07$	-0.06 ± 0.02
[Cr I/Fe]	$+0.01 \pm 0.04$	-0.01 ± 0.02
[Fe I/H]	-0.33 ± 0.05	-0.26 ± 0.03
[Fe II/H]	-0.33 ± 0.06	-0.26 ± 0.03
[Ni I/Fe]	-0.06 ± 0.01	-0.07 ± 0.02

the stars of thin disc and with metallicities between -0.3 and -0.4 is $+0.12 \pm 0.05$ (Luck & Heiter 2007).

We could not obtain the abundance of titanium in NGC 2345-60 due to severe blending of the lines, which made the determination of this abundance very uncertain. Also, due to this exclusion this star presents high abundance in α-elements. For [Al/Fe], we also find the typical value for disc field giants from Luck & Heiter (2007) in the same metallicity range.

We also observed a low abundance of the iron-peak elements, a fact that was already expected due to low metallicity of the open cluster NGC 2345. The abundance ratios [Cr/Fe] and [Ni/Fe] follow the same trend with iron abundance ([X/Fe] is close to zero). In addition also, a low [Ni/Fe] ratio was found, below the pattern found by Luck & Heiter (2007) for objects with the same metallicity but still within the observed pattern for red clump giants studied by Mishenina et al. (2006). The average of [Ni/Fe] for our giants is -0.06 ± 0.01, which is very close to that found by Reddy et al. (2016) for a smaller number of stars (-0.07 ± 0.02).

Finally, we present in Table 7 a comparison between the abundances determined by Reddy et al. (2016) and our results. In general, the discrepancy is small, since the mean difference between the two works is 0.05 ± 0.07.

4.2.4 Heavy elements: the neutron-capture elements

Fig. 15 shows the abundance ratios ([X/Fe]) for the s-process elements for the giants of NGC 2345 in comparison with the same elements studied by Luck & Heiter (2007) and Mishenina et al. (2006). We also show the mean abundance of the s-process elements as defined in Section 3.2 for NGC 2345 and for the two samples of field giant stars above mentioned. Fig. 15 shows that NGC 2345 presents a small enrichment of the mean s-process abundances compared to the field giant stars. In this context, we denote that young open clusters are not only more s-process enriched than older open clusters, as first noticed by Maiorca et al. (2012), but are also more enriched the field stars.

The top panels in Fig. 16 show samarium and europium abundances of the giants analysed in this work in comparison with the dwarfs and subgiants analysed by Luck (2017) (for samarium) and with the field giants analysed by Luck & Heiter (2007) and Mishenina et al. (2006) (for europium). The abundances of samarium and europium are in good agreement with the sample of Luck (2017) and Mishenina et al. (2006), respectively. The bottom panel of Fig. 16 shows the mean europium abundance of NGC 2345 and the mean europium abundance of other open clusters analysed in other

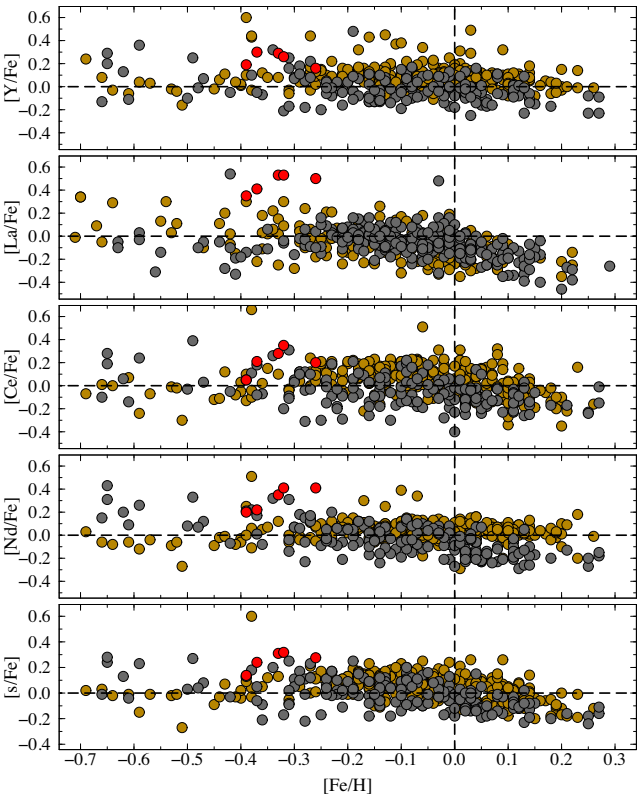

Figure 15. Abundance ratios [X/Fe] versus [Fe/H] for the elements from Y to Nd. The bottom frame is the mean value of the s-elements, [s/Fe]. Symbols have the same meaning as in Fig. 10.

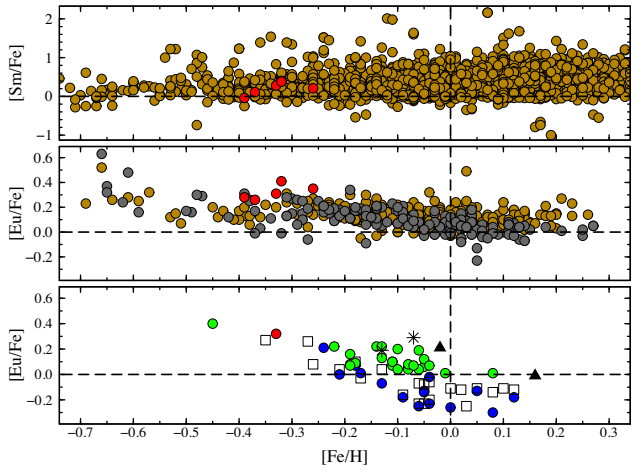

Figure 16. Samarium- and europium-over-iron versus iron abundances for field stars (top panels) and open clusters from other studies (bottom panel) for the average [Eu/Fe] abundances. In top panels, we present data from Luck (2017) and Luck & Heiter (2007) (yellow) and Mishenina et al. (2006) (grey). In bottom panel open squares were taken from Jacobson & Friel (2013), green filled circles from Reddy et al. (2012, 2013, 2015, 2016), blue filled circles from Overbeek et al. (2016), black triangles from Drazdauskas et al. (2016), and asterisks from Začs et al. (2011).

Table 8. Comparison of the heavy-element abundance ratios [X/Fe] for NGC 2345 derived in this study and in Reddy et al. (2016). The values in Reddy et al. (2016) are based on the abundances of stars #34, #43, and #60.

Species	This work	Reddy et al. (2016)
[Y II/Fe]	$+0.24 \pm 0.06$	$+0.16 \pm 0.02$
[Zr I/Fe]	$+0.04 \pm 0.08$	-0.05 ± 0.03
[La II/Fe]	$+0.46 \pm 0.08$	$+0.01 \pm 0.02$
[Ce II/Fe]	$+0.22 \pm 0.11$	$+0.02 \pm 0.02$
[Nd II/Fe]	$+0.32 \pm 0.10$	$+0.03 \pm 0.02$
[Sm II/Fe]	$+0.19 \pm 0.16$	$+0.12 \pm 0.02$
[Eu II/Fe]	$+0.32 \pm 0.06$	$+0.12 \pm 0.05$

works. The abundance of europium in NGC 2345 is in agreement with the results found in literature, despite the small amount of data for low metallicities (i.e. [Fe/H] < -0.25). For this comparison, we compiled data from Začs et al. (2011), Jacobson & Friel (2013), Reddy et al. (2012, 2013, 2015, 2016), Drazdauskas et al. (2016), and Overbeek, Friel & Jacobson (2016).

Table 8 shows individual abundances for comparison purposes with Reddy et al. (2016) results. Larger discrepancies occur in the abundances of heavy elements (mean difference of 0.20 ± 0.14). We assign this discrepancy to the number of lines used, uncertainty in determining the continuum, and different atmospheric parameters. Nevertheless, the giants analysed here have a similar abundance profile to those of the red clump stars analysed by Mishenina et al. (2006).

5 CONCLUSIONS

The main conclusions of our abundance analysis employing high-resolution optical spectra of the five giants of the open cluster NGC 2345 can be summarized as follows.

(i) NGC 2345 is a very young open cluster with a turn-off mass of $5.4 \pm 0.15\,M_{\odot}$. The metallicity for this open cluster is low ([Fe/H] $= -0.33$) for its Galactic latitude ($-02^{\circ}31$). Compared to other massive clusters of similar age, such as NGC 1545 (Začs et al. 2011) and NGC 5316 (Drazdauskas et al. 2016), NGC 2345 still appears peculiar in its metallicity. This was confirmed by analysis of the radial gradient of metallicity, where NGC 2345 stands out together with another very young cluster, NGC 3105 (28 Myr; Alonso-Santiago et al. 2018).

(ii) We determined rotational velocities for all the known giants of NGC 2345 using spectral synthesis method. NGC 2345 – 34 presents high projected rotational velocity ($v \sin i = 10.1\,\mathrm{km\,s^{-1}}$) that can be attributed to a well-known binarity of this star, evidenced here by its radial velocity compared to the other reports from the literature. In addition, we noticed a scarcity a lithium abundance determination for giants in massive clusters, those with low $\log g$.

(iii) The abundance of sodium and the $^{12}C/^{13}C$ isotopic ratio found for NGC 2345 are similar to the values predicted by the standard models by Lagarde et al. (2012). The values found for these mixing tracers are also very close to that of reported by Drazdauskas et al. (2016) in their study of clusters NGC 4609 and NGC 5316 of similar turn-off masses.

(iv) Finally, the results for C and N for the five giants show a post-first dredge-up profile. Furthermore, there is good agreement between our results and those presented by Mishenina et al. (2006) for abundances of the n-capture elements in red clump giants.

ACKNOWLEDGEMENTS

NH thanks the Coordenação de Aperfeiçoamento de Pessoal de Nível Superior (CAPES) for financial support, grant 88882.184153/2018-01. NAD acknowledges financial support by Russian Foundation for Basic Research (RFBR) according to the research projects 18-02-00554 and 18-02-06004. The use of the SIMBAD, VizieR, CDS Portal, and WEBDA is acknowledged.

REFERENCES

Alonso A., Arribas S., Martínez-Roger C., 1999, A&AS, 140, 261
Alonso-Santiago J., Marco A., Negueruela I., Tabernero H., Castro N., McBride V. A., Rajoelimanana A., 2018, A&A, 616, A124
Asplund M., Grevesse N., Sauval A. J., Scott P., 2009, ARA&A, 47, 481
Bauschlicher C. W., Langhoff S. R., Taylor P. R., 1988, ApJ, 332, 531
Bertelli G., Bressan A., Chiosi C., Fagotto F., Nasi E., 1994, A&AS, 106, 275
Carlberg J. K., Majewski S. R., Patterson R. J., Bizyaev D., Smith V. V., Cunha K., 2011, ApJ, 732, 39
Cayrel R., 1988, in Cayrel de Strobel G.,Spite M., eds, Proc. IAU Symp. 132, The Impact of Very High S/N Spectroscopy on Stellar Physics. Kluwer, Dordrecht, p. 345
Charbonnel C., Balachandran S., 2000, A&A, 359, 563
Charbonnel C., Lagarde N., 2010, A&A, 522, A10
da Silveira M., Pereira C., Drake N., 2018, MNRAS, 476, 4907
Davis S. P., Phillips J. G., 1963, The Red System of the CN Molecule. Univ. California Press, Berkley, CA
Delgado-Mena E. et al., 2016, A&A, 587, A66
Dias W., Alessi B., Moitinho A., Lépine J., 2002, A&A, 389, 871
Drazdauskas A., Tautvaišienė G., Smiljanic R., Bagdonas V., Chorniy Y., 2016, MNRAS, 462, 794
Dwivedi P. H., Branch D., Huffaker J. N., Bell R. A., 1978, ApJS, 36, 573
Fekel F. C., 1997, PASP, 109, 514
Friel E., 1995, ARA&A, 33, 381
Gaia Collaboration et al., 2018, A&A, 616, A1
Genovali K. et al., 2013, A&A, 554, A132
Genovali K. et al., 2014, A&A, 566, A37
Gilroy K. K., 1989, ApJ, 347, 835
Heiter U., Soubiran C., Netopil M., Paunzen E., 2014, A&A, 561, A93
Hekker S., Meléndez J., 2007, A&A, 475, 1003
Huber K. P., Herzberg G., 1979, Molecular Spectra and Molecular Structure, IV: Constants of Diatomic Molecules. Van Nostrand Reinhold, New York
Jacobson H. R., Friel E. D., 2013, AJ, 145, 107
Karakas A. I., Lattanzio J. C., 2014, Publ. Astron. Soc. Aust., 31, e030
Kaufer A., Stahl O., Tubbesing S., Nørregaard P., Avila G., Francois P., Pasquini L., Pizzella A., 1999, The Messenger, 95, 8
Kharchenko N., Piskunov A., Röser S., Schilbach E., Scholz R.-D., 2005, A&A, 438, 1163
Kovács I., 1969, Rotational Structure in the Spectra of Diatomic Molecules. Adam Hilger, London
Kurucz R. L., 1993, Kurucz CD-Rom. Smithsonian Astrophysical Observatory, Cambridge, MA
Lada C. J., Lada E. A., 2003, ARA&A, 41, 57
Lagarde N., Decressin T., Charbonnel C., Eggenberger P., Ekström S., Palacios A., 2012, A&A, 543, A108
Lambert D. L., 1978, MNRAS, 182, 249
Lambert D. L., 1994, in Jorgensen U. G., ed., Lecture Notes in Physics, Vol. 428, IAU Colloq. 146, Molecules in the Stellar Environment. Springer-Verlag, Berlin, p. 1
Luck R. E., 2017, AJ, 153, 21
Luck R. E., Heiter U., 2007, AJ, 133, 2464
Maiorca E., Magrini L., Busso M., Randich S., Palmerini S., Trippella O., 2012, ApJ, 747, 53
Meléndez J., Barbuy B., 1999, ApJS, 124, 527
Mermilliod J., Mayor M., Udry S., 2008, A&A, 485, 303

Mishenina T., Bienaymé O., Gorbaneva T., Charbonnel C., Soubiran C., Korotin S., Kovtyukh V., 2006, A&A, 456, 1109
Moffat A., 1974, A&AS, 16, 33
Mucciarelli A., Caffau E., Freytag B., Ludwig H.-G., Bonifacio P., 2008, A&A, 484, 841
Netopil M., Paunzen E., Heiter U., Soubiran C., 2016, A&A, 585, A150
Overbeek J. C., Friel E. D., Jacobson H. R., 2016, ApJ, 824, 75
Peña-Suárez V., Silva J. S., Santrich O. K., Drake N., Pereira C., 2018, ApJ, 854, 184
Phillips J. G., Davis S. P., 1968, The Swan System of the C2 Molecule. Univ. California Press, Berkley, CA
Reddy A. B., Giridhar S., Lambert D. L., 2012, MNRAS, 419, 1350
Reddy A. B., Giridhar S., Lambert D. L., 2013, MNRAS, 431, 3338
Reddy A. B., Giridhar S., Lambert D. L., 2015, MNRAS, 450, 4301
Reddy A. B., Lambert D. L., Giridhar S., 2016, MNRAS, 463, 4366
Sales Silva J., Suárez V. P., Santrich O. K., Pereira C., Drake N., Roig F., 2014, AJ, 148, 83
Santos N., Lovis C., Pace G., Melendez J., Naef D., 2009, A&A, 493, 309
Santrich O. K., Pereira C., Drake N., 2013, A&A, 554, A2
Schadee A., 1964, Bull. Astron. Inst. Netherlands, 17, 311
Sneden C., 1973, PhD thesis. Univ. Texas at Austin
Sneden C., Lambert D., 1982, ApJ, 259, 381
Stephenson C. B., Sanduleak N., 1971, Publ. Warner & Swasey Obser., 1, 1
Takeda Y., Sato B., Murata D., 2008, PASJ, 60, 781
Wyller A. A., 1966, ApJ, 143, 828
Yong D., Carney B. W., Friel E. D., 2012, AJ, 144, 95
Začs L., Alksnis O., Barzdis A., Laure A., Musaev F., Bondar A., Sperauskas J., 2011, MNRAS, 417, 649
Zieliński P., Niedzielski A., Wolszczan A., Adamów M., Nowak G., 2012, A&A, 547, A91

APPENDIX: EXTRA MATERIAL

Table A1. Observed Fe I and Fe II lines. The column for each star shows the equivalent width in units of mÅ.

				Equivalent widths (mÅ) NGC 2345 – #				
Element	λ (Å)	χ (eV)	log *gf*	14	34	43	50	60
Fe I	5775.080	4.220	− 1.300	119	116	112	113	120
	5848.129	4.607	− 0.900	102	80	97	108	106
	5902.473	4.593	− 1.750	43	–	42	40	37
	6027.050	4.076	− 1.300	131	141	124	126	130
	6093.644	4.607	− 1.410	65	64	69	71	–
	6096.665	3.984	− 1.810	92	76	85	91	93
	6098.244	4.558	− 1.800	59	45	–	–	–
	6120.249	0.915	− 5.950	119	46	99	131	133
	6151.618	2.176	− 3.300	–	146	–	–	–
	6187.990	3.943	− 1.650	112	91	109	110	113
	6574.228	0.990	− 5.000	–	143	–	–	–
	6703.567	2.759	− 3.150	132	114	127	144	140
	6725.357	4.103	− 2.300	65	40	59	61	63
	6726.666	4.607	− 1.170	88	85	90	82	86
	7421.558	4.638	− 1.800	43	31	39	56	46
	7547.896	5.099	− 1.100	45	–	40	44	44
	7723.208	2.279	− 3.620	–	133	144	–	–
Fe II	5264.812	3.230	− 3.130	–	140	63	–	53
	5425.257	3.200	− 3.220	–	128	68	57	54
	6247.557	3.892	− 2.300	58	–	–	–	–
	6369.462	2.891	− 4.110	41	92	38	39	35
	6432.680	2.891	− 3.570	71	143	70	–	59
	6456.383	3.904	− 2.050	68	–	80	64	64

Table A2. Observed lines of other elements. The column for each star shows the equivalent width in units of mÅ.

				Equivalent widths (mÅ) NGC 2345 – #				
Element	λ (Å)	χ (eV)	log *gf*	14	34	43	50	60
Na I	4751.820	2.100	– 2.095	83	47	–	90	77
	5148.840	2.100	– 2.095	75	–	–	–	–
	6154.220	2.100	– 2.095	130	82	102	130	–
	6160.750	2.100	– 1.261	–	108	112	144	141
Mg I	4730.040	4.340	– 2.390	–	–	114	118	107
	6319.240	5.110	– 2.160	61	–	–	–	–
	6319.490	5.110	– 2.670	30	–	–	–	–
	7387.700	5.750	– 0.870	95	–	–	–	–
	8712.690	5.930	– 1.260	–	–	85	–	75
	8717.830	5.910	– 0.970	103	97	89	100	106
	8736.040	5.940	– 0.340	132	143	–	148	145
Al I	6698.670	3.140	– 1.630	104	52	77	103	96
	7835.320	4.040	– 0.580	–	83	–	89	92
	7836.130	4.020	– 0.400	111	82	92	105	107
	8772.880	4.020	– 0.250	121	123	116	124	121
	8773.910	4.020	– 0.070	–	–	135	–	145
Si I	5793.080	4.930	– 2.060	74	90	78	73	69
	6125.030	5.610	– 1.540	–	57	–	–	–
	6131.577	5.620	– 1.685	32	–	37	28	–
	6145.020	5.610	– 1.430	46	–	49	40	43
	6155.140	5.620	– 0.770	95	116	100	88	93
	7760.640	6.200	– 1.280	–	–	–	18	–
	7800.000	6.180	– 0.720	–	78	–	–	–
	8728.010	6.180	– 0.360	59	–	70	44	72
	8742.450	5.870	– 0.510	95	–	–	92	–
Ca I	5867.572	2.930	– 1.610	84	41	71	84	79
	6166.440	2.520	– 1.140	147	135	–	–	–
	6455.600	2.510	– 1.290	–	126	139	–	–
	6464.680	2.520	– 2.420	–	–	–	–	108
	6798.467	2.710	– 2.520	58	15	32	60	46
Ti I	4778.260	2.240	– 0.330	103	44	92	117	–
	4820.410	1.500	– 0.440	–	141	–	–	–
	5009.660	0.020	– 2.260	–	126	–	–	–
	5062.100	2.160	– 0.460	–	44	90	–	–
	5223.630	2.090	– 0.561	114	–	95	–	–
	5295.780	1.050	– 1.631	–	62	–	–	–
	5503.900	2.580	– 0.190	–	–	–	124	–
	5689.480	2.300	– 0.470	107	–	85	118	–
	5922.120	1.050	– 1.470	–	113	–	–	–
	6091.180	2.270	– 0.420	127	56	93	138	–
	6126.220	1.070	– 1.420	–	108	–	–	–
	6554.240	1.440	– 1.220	–	72	126	–	–
Cr I	4790.340	2.544	– 1.480	92	–	–	105	–
	4870.800	3.078	– 0.010	–	115	–	–	–
	4887.680	2.543	– 2.071	58	–	42	65	–
	4936.340	3.112	– 0.250	118	73	101	129	–
	4953.710	3.120	– 1.480	–	–	–	70	37
	5067.720	2.708	– 1.070	–	60	–	–	–
	5144.660	2.709	– 1.371	106	49	–	–	94
	5200.210	3.384	– 0.580	–	–	–	–	103
	5238.960	2.708	– 1.270	85	34	–	93	–
	5241.450	2.709	– 1.921	–	–	36	61	–
	5265.160	3.427	– 0.350	–	–	93	–	113
	5272.010	3.448	– 0.420	–	–	74	86	–
	5287.200	3.437	– 0.870	73	–	46	75	61
	5304.180	3.462	– 0.670	–	34	–	–	–
	5312.870	3.448	– 0.550	–	37	–	70	–
	5344.790	3.448	– 0.990	–	–	38	–	–
	5628.620	3.420	– 0.740	64	–	55	71	–
	5664.040	3.434	– 0.710	92	58	79	92	–
	5712.750	3.010	– 1.030	–	–	–	107	–
	5719.810	3.012	– 1.580	58	–	38	64	46

Table A2 – *continued*

Element	λ (Å)	χ (eV)	log *gf*	Equivalent widths (mÅ) NGC 2345 – # 14	34	43	50	60
	5787.040	3.012	– 1.551	–	–	45	67	–
	5838.650	3.010	– 1.821	–	–	–	68	45
	5844.590	3.012	– 1.772	59	–	42	67	–
	5884.430	3.012	– 1.860	59	–	37	55	–
Ni I	4913.980	3.740	– 0.600	–	–	–	97	–
	4953.210	3.740	– 0.580	–	110	–	–	–
	4967.520	3.800	– 1.600	–	–	–	52	–
	5003.750	1.677	– 3.070	–	–	110	–	–
	5010.940	3.635	– 0.979	95	96	94	–	–
	5084.110	3.677	– 0.180	–	–	–	118	–
	5157.980	3.606	– 1.510	59	–	–	–	53
	5388.344	1.935	– 3.510	–	61	–	–	–
	5435.856	1.986	– 2.580	–	128	–	–	–
	5748.360	1.677	– 3.240	–	–	109	–	–
	6007.310	1.677	– 3.400	–	88	105	–	–
	6086.290	4.270	– 0.470	–	–	–	76	–
	6111.080	4.090	– 0.830	–	–	–	69	–
	6128.980	1.677	– 3.429	–	105	–	–	–
	6176.820	4.089	– 0.260	106	110	99	107	99
	6177.250	1.826	– 3.460	–	66	86	99	97
	6186.720	4.110	– 0.900	–	–	–	73	–
	6204.610	4.089	– 1.080	70	52	57	72	73
	6223.990	4.106	– 0.910	59	–	60	60	70
	6327.600	1.677	– 3.170	–	136	–	–	–
	6378.260	4.154	– 0.821	–	–	78	–	–
	6532.873	1.945	– 3.350	–	97	–	–	–
	6586.320	1.951	– 2.780	148	116	–	–	–
	6772.320	3.660	– 1.013	–	–	–	116	–
Y II	5200.415	0.990	– 0.570	156	–	143	163	–
	5289.815	1.030	1.850	56	72	54	63	50
	5402.783	1.840	– 0.440	95	104	72	100	91
Zr I	4772.300	0.620	– 0.060	116	22	82	131	–
	4784.940	0.690	– 0.600	69	–	44	97	66
	4805.870	0.690	– 0.580	72	–	41	83	–
	4828.050	0.620	– 0.750	74	–	40	91	79
	5046.550	1.530	– 0.180	–	–	17	–	–
	5385.130	0.520	– 0.640	91	13	53	107	–
	5437.770	0.150	– 2.120	–	–	–	63	35
	5620.130	0.520	– 1.090	79	–	47	88	67
	5885.620	0.070	– 1.730	69	–	27	80	–
	6032.600	1.480	– 0.350	35	–	–	45	24
	6127.460	0.150	– 1.060	130	23	84	150	–
	6134.570	0.000	– 1.280	122	16	74	146	–
	6140.460	0.520	– 1.410	55	–	24	67	41
	6143.180	0.070	– 1.100	140	31	–	–	–
La II	4934.830	1.250	– 0.920	–	36	–	–	–
	5303.530	0.320	– 1.350	82	–	71	86	77
	5880.630	0.235	– 1.830	65	–	48	75	–
	6320.429	0.170	– 1.520	107	–	85	115	100
	6390.480	0.320	– 1.410	103	96	75	–	89
	6774.330	0.120	– 1.709	109	98	82	108	103
Ce II	4486.909	0.295	– 0.180	–	–	–	–	123
	4562.370	0.480	0.210	–	–	–	–	122
	4628.160	0.520	0.140	130	–	–	–	125
	5187.457	1.211	0.170	90	79	68	–	71
	5274.236	1.044	0.130	77	94	71	–	75
	5330.580	0.869	– 0.400	72	68	–	–	64
	5975.818	1.326	– 0.450	–	–	26	–	–
	6043.373	1.205	– 0.480	–	43	31	–	–
Nd II	4706.540	0.000	– 0.710	119	124	104	–	–
	4709.720	0.182	– 0.970	–	119	–	–	–
	4763.620	0.380	– 1.270	–	–	–	56	50
	4777.720	0.380	– 1.220	–	94	–	–	–

Table A2 – *continued*

Element	λ (Å)	χ (eV)	log *gf*	Equivalent widths (mÅ) NGC 2345 – # 14	34	43	50	60
	4797.150	0.559	– 0.690	–	–	–	77	75
	4859.030	0.320	– 0.440	–	–	–	–	111
	4914.380	0.380	– 0.699	–	–	99	–	97
	4959.119	0.320	– 0.800	–	135	–	–	–
	4987.160	0.742	– 0.790	–	–	54	72	–
	5063.722	0.976	– 0.620	–	42	–	–	57
	5092.800	0.380	– 0.610	–	100	85	93	91
	5212.361	0.200	– 0.960	–	108	–	–	–
	5306.460	0.859	– 0.970	–	–	–	–	44
	5311.460	0.980	– 0.420	–	96	–	–	–
	5356.970	1.263	– 0.280	45	–	–	52	45
	5485.700	1.263	– 0.120	71	76	69	75	65
	5740.875	1.160	– 0.530	53	45	41	54	52
	5811.570	0.859	– 0.860	57	–	42	60	49
Sm II	4478.654	0.659	– 0.360	–	85	–	–	–
	4499.475	0.248	– 0.870	80	–	–	–	65
	4536.510	0.104	– 1.280	–	49	–	–	–
	4566.202	0.333	– 0.590	90	–	75	90	–
	4642.230	0.380	– 0.460	–	–	–	–	75
	4676.900	0.040	– 0.870	102	91	–	106	89
	4704.400	0.000	– 0.860	108	–	89	112	97
	4791.600	0.100	– 1.440	–	–	62	–	–

This paper has been typeset from a TEX/LATEX file prepared by the author.